Supporting Information

Fluorinating Dopant-free Small-molecule Hole-transport Material to Enhance the Photovoltaic Property

*Yikai Wang[a, ‡], Hui Ma[b, ‡], Qiaoyun Chen[b], Quan Sun[a], Zhengxu Liu[a], Zhe Sun[a], Xuguang Jia[a], Yuanyuan Zhu[a], Shuai Zhang[a], Jing Zhang[a, *], Ningyi Yuan[a, *], Jianning Ding[a], Yi Zhou[b, *], Bo Song[b, *], and Yongfang Li[b]*

Contents

1. Experimental section

1.1 Materials synthesis

All reagents were obtained from Beijing InnoChem Science&Technology Co. Ltd, Sun Chemical Technology(Shanghai) Co. Ltd, Xi'an Polymer Light Technology Corp. and Solarmer Materials Inc., respectively. The synthetic routes, mass and NMR spectra of BT-MTP and DFBT-MTP are as follows.

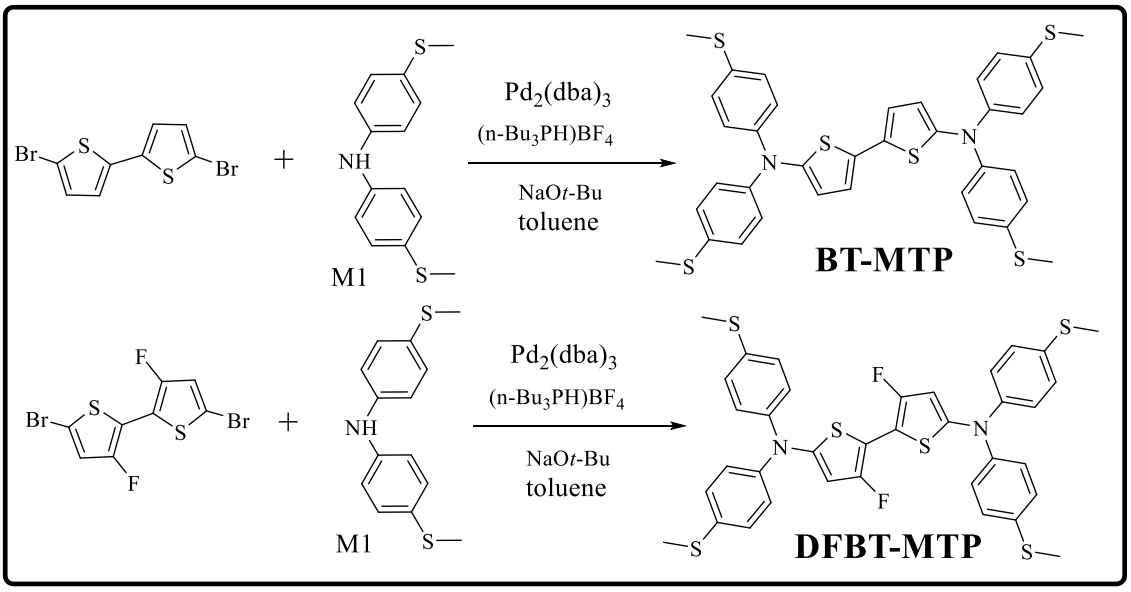

Scheme S1. Synthetic routes of BT-MTP and DFBT-MTP.

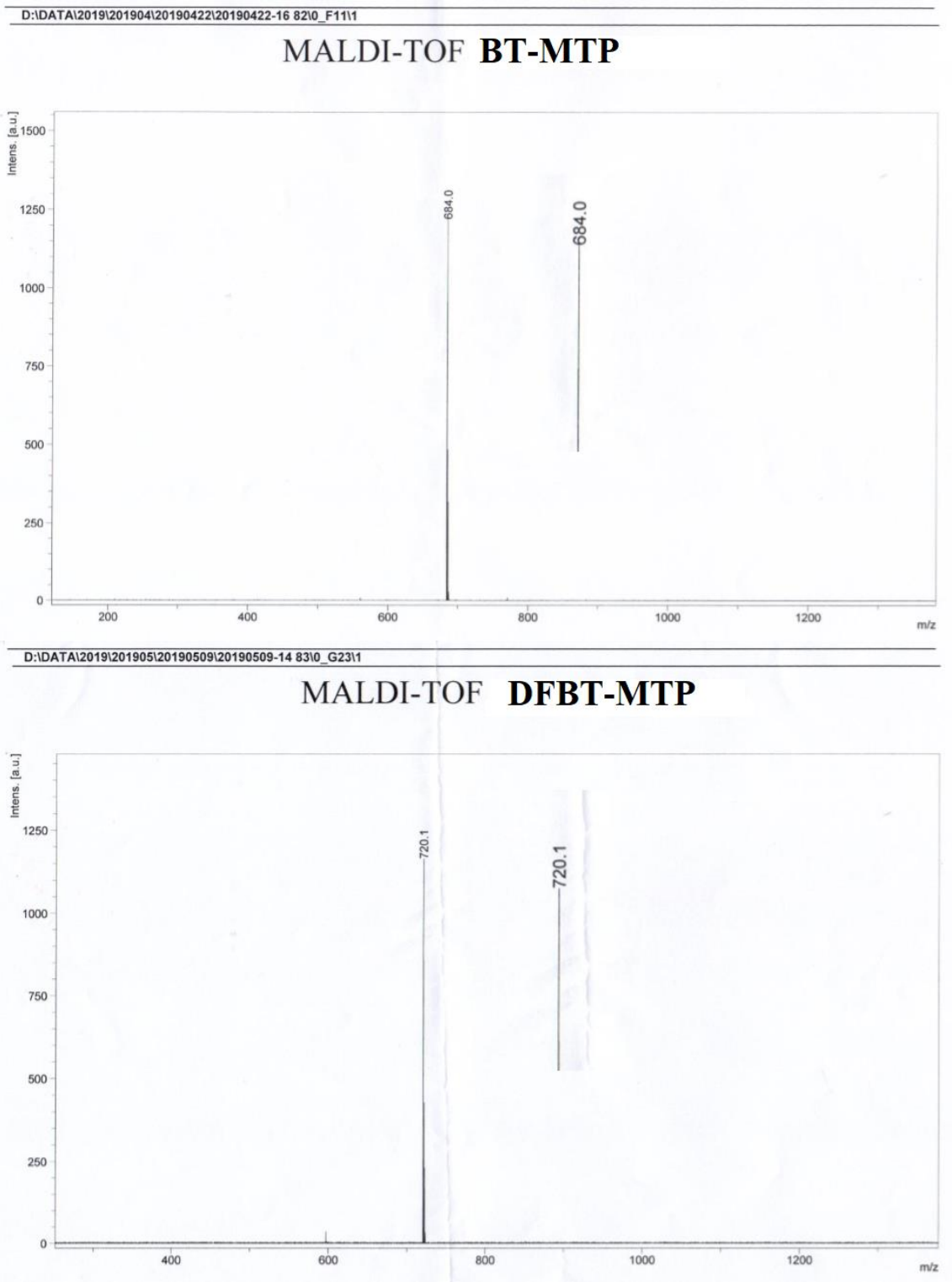

Figure S1. MALDI-TOF mass spectrometry of BT-MTP and DFBT-MTP.

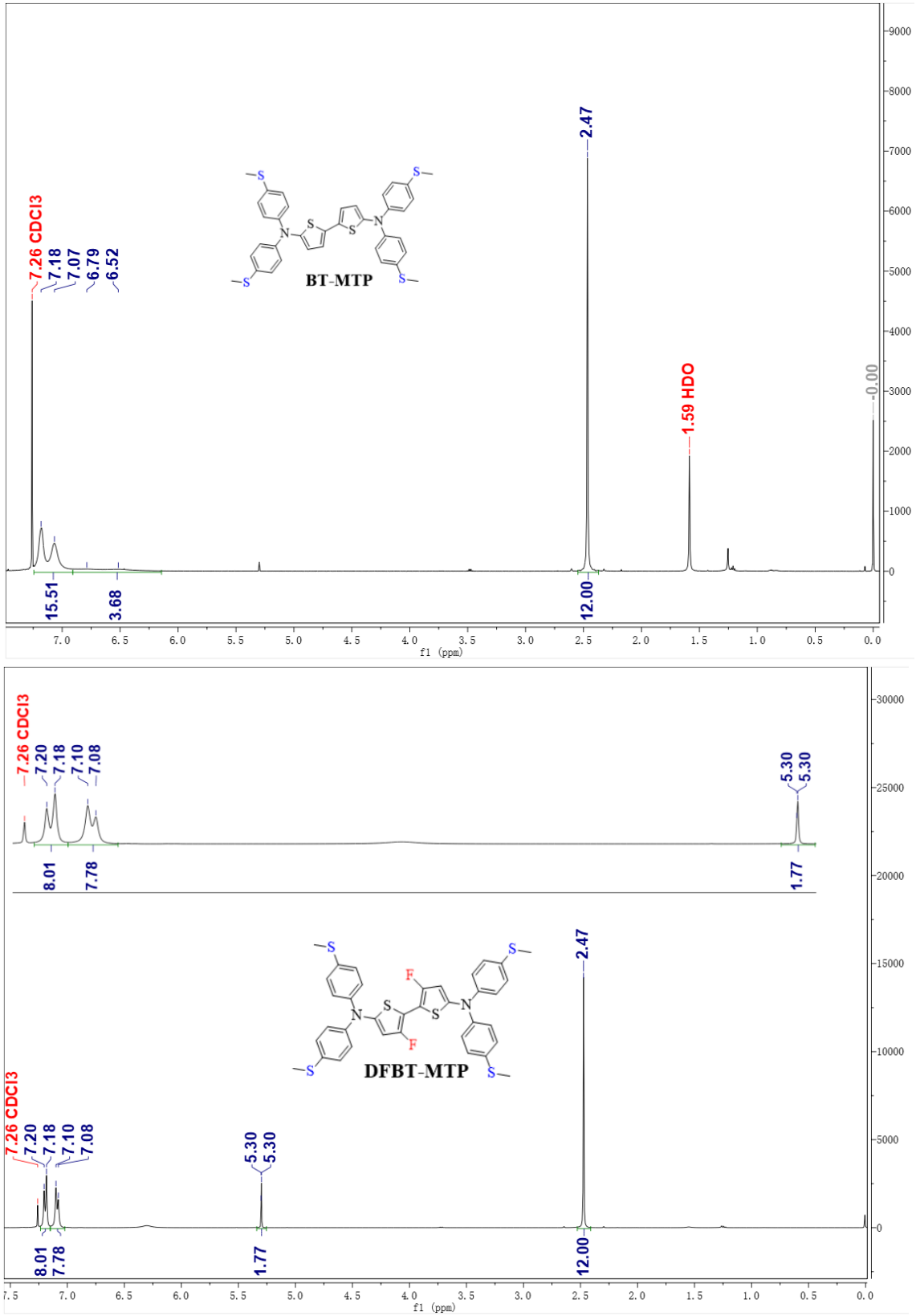

Figure S2. ^{1}H NMR spectra of BT-MTP and DFBT-MTP.

1.2 Measurements and instruments

MALDI-TOF spectra, NMR spectra, absorption spectra and the electrochemical cyclic voltammogram were recorded on Bruker BIFLEX III, Bruker DMX-500, Hitachi U-3010 UV-vis spectrophotometer and Zahner IM6e electrochemical workstation, respectively. The CV measurement taken with a platinum sheet, platinum wire, and Ag/Ag^+ electrode as working electrode, counter electrode, and reference electrode, respectively. The CV tests were conducted in a 0.1 M chloroform solution of Bu_4NPF_6. During the measurement, ferrocene/ferrocenium (Fc/Fc^+) was used as an internal standard, which was assigned an absolute energy of 4.74 eV versus vacuum level. The thermal stability was measured on HTG-1. The FTIR Spectra were measured on Nicolet-460. The XRD spectra were tested on D2 PHASER (Bruker, Germany). The XPS spectra were tested on Thermo Escalab 250Xi X-ray photoelectron spectrometer using 300W Al Kα radiation under a pressure of $\sim 3\times10^{-9}$ mbar. The SEM images were tested on Dimension V and SUPRA8010, respectively. The *J-V* curves of PVK-SCs were recorded using a Keithley 2400 source meter in a glove box filled with N^2. The measurement was conducted under AM 1.5G solar illumination with an intensity of 100 mW cm^{-2} at a scan speed of 10 mV s^{-1}. Shadow masks were clung to the substrate to define an active area of 0.0757 cm^2. A solar simulator (500 W Xe lamp) (ORIEL Solar 3A94023A, America) is employed as the light source. The EQE curves were calibrated by using a solar cell spectral response measurement system (Enli Technology Co., Ltd, QE-R3011) in atmosphere conditions. Steady-state photoluminescence (PL) spectra were carried out on FLS 980 (Edinburgh Instrument, UK). Time-resolved PL measurements were acquired on Lifespec II (Edinburgh Instrument, UK). The Nyquist tests were carried out by an IM6 electrochemical workstation (Zahner Zennium, Germany) in the dark with a bias under the respective *V*oc of individual cells. All the devices were measured immediately after fabricated.

1.3 Device fabrication

ITO glass substrates were ultrasonically cleaned with deionized water, ethanol, acetone and isopropanol for 30 min, respectively, then dried with N_2. Then followed by oxygen plasma cleaning for 20 min before using. The synthesized HTL materials (BT-MTP and DFBT-MTP) was dissolved in CB with a concentration of 10 mg mL^{-1}. Then, it was spin-coated on the ITO/glass substrates at a speed of 5000 rpm for 35 s. The resulting HTL film was thermally annealed at 100 ℃ for 5 min. The perovskite layer was fabricated by a two-step method. PbI_2 precursor solution (Concentration of 1 mole/ml, dissolved in DMF) was stirred at 70 ℃ overnight on a hot plate. MAI precursor solution (MAI: MACl=10:1, 50 mg mL^{-1}, dissolved in isopropanol) On the top of the HTL, the PbI_2 precursor solution was firstly spin-coated at 3500 rpm for 20 s. Then MAI and MACl mixed solution was spin-coated at 3500 rpm for 30 s above PbI_2 film. After that, the deposited films were thermally annealed at 90 ℃ for 8 min in a nitrogen-filled glove-box. Then the $MAPbI_{3-x}Cl_x$-based perovskite is formed. Because of the annealing process, parts of MACl were volatilized. We used thermally evaporated C_{60}/BCP (2,9-Dimethyl-4,7-diphenyl-1,10-phenanthroline) double layers as cathode buffer layer in the device by vacuum evaporation under 2×10^{-4} mbar; we considered that the BCP film as an electron-transporting and hole-blocking layer could realize enhancement of device performance. Finally, an Ag (800 nm) electrode was deposited on the BCP by vacuum evaporation under 2×10^{-6} mbar. The device structure is ITO/DBTMT/$MAPbI_{3-x}Cl_x$/ C_{60} (20 nm)/ BCP (8 nm)/Ag.

2. DFT-calculation

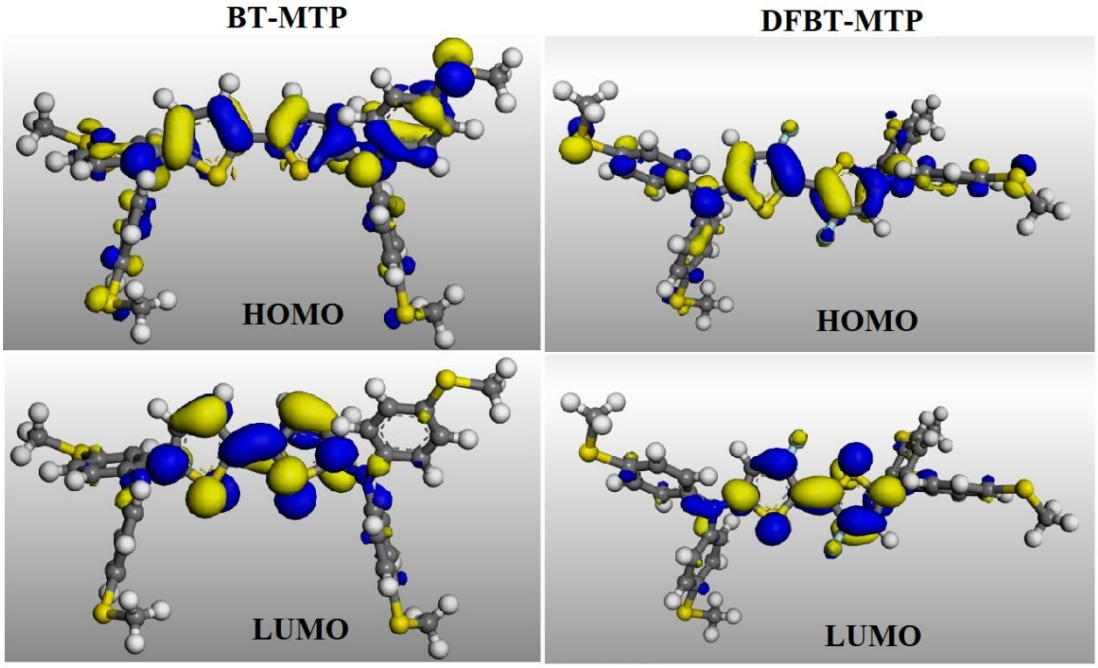

Figure S3. The DFT-calculated electronic structures, showing the HOMO and LUMO energy levels of BT-MTP and DFBT-MTP.

3. The thermal, optical and electrical properties

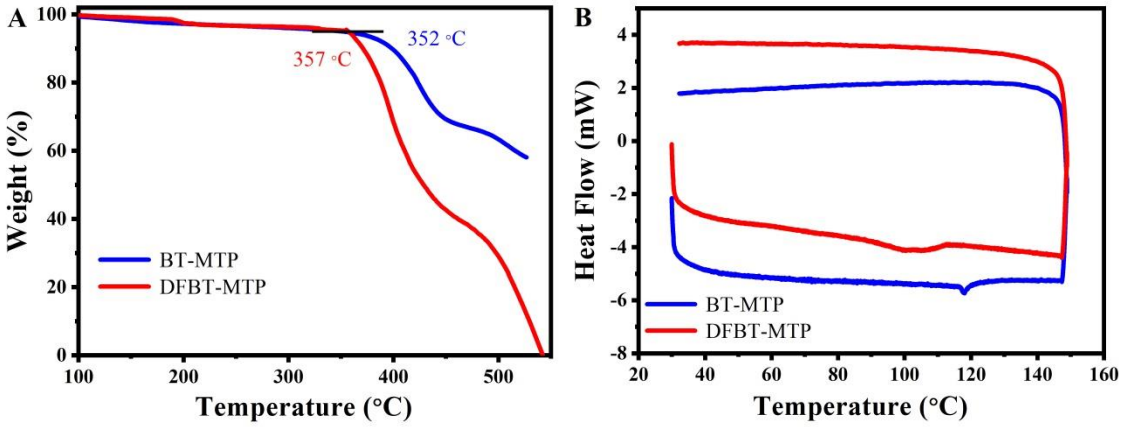

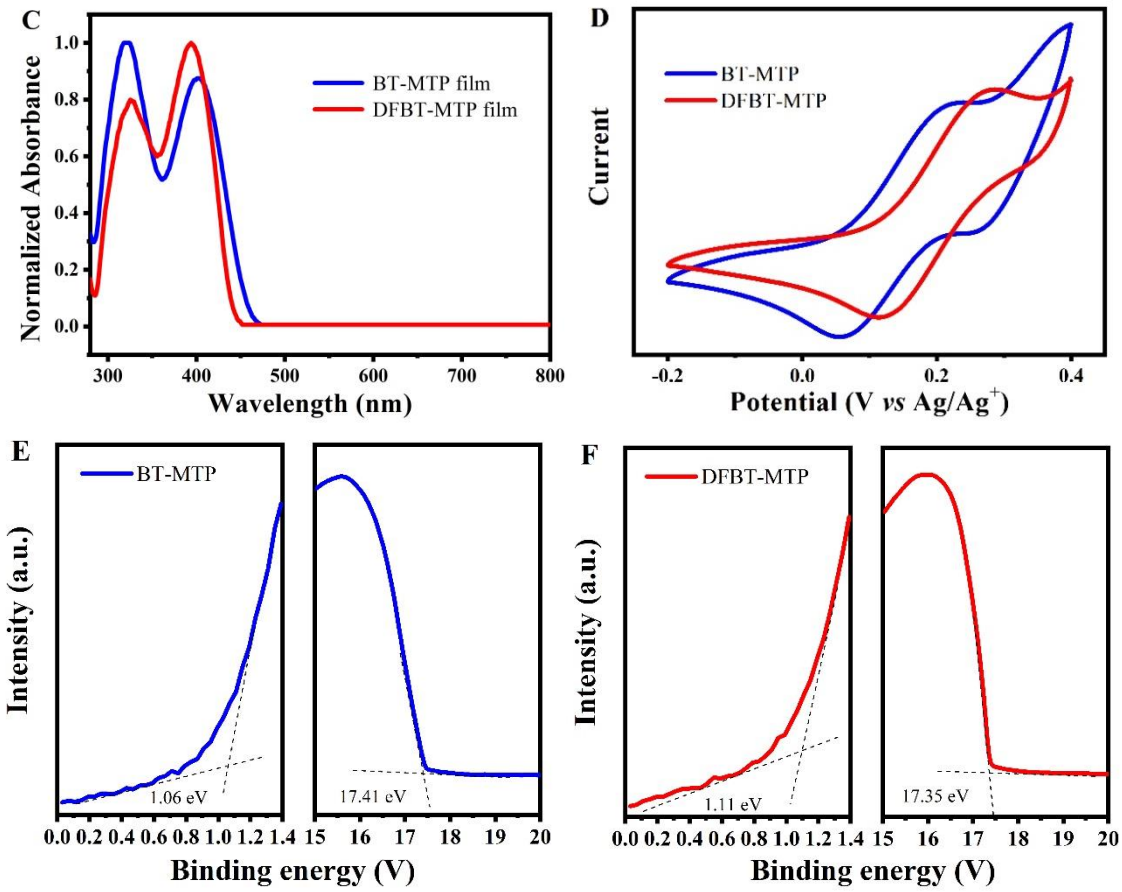

Figure S4. The TGA plots (A), the DSC plots (B), the UV-vis spectra (C), Cyclic voltammogram (D), UPS spectra (E, F) of BT-MTP and DFBT-MTP, respectively.

4. Contact Angles

Table S1. The five times and average DMF droplets contact angles on the surface of the BT-MTP and DFBT-MTP film.

	1	2	3	4	5	Average
BT-MTP	6 °	7 °	10.5 °	9.5 °	9 °	8.4 °
DFBT-MTP	7 °	9 °	10.5 °	7.5 °	8.5 °	8.5 °

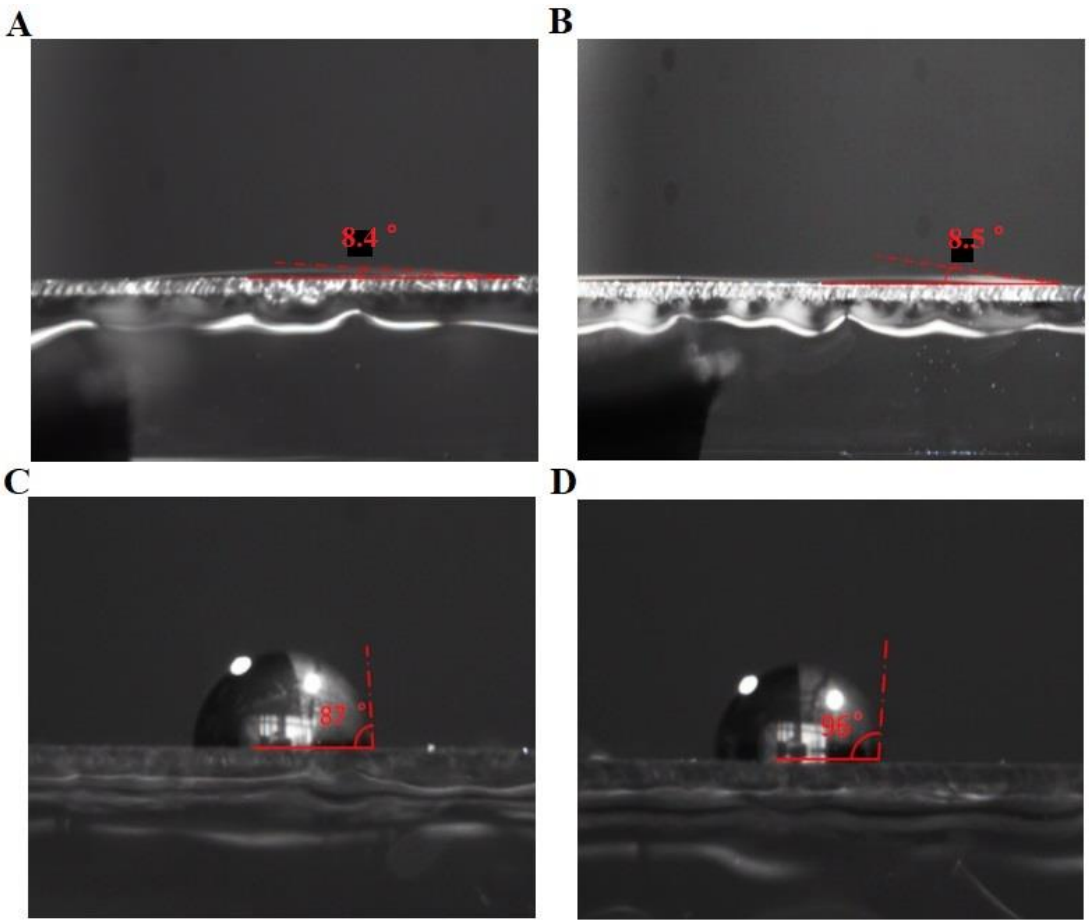

Figure S5. Images of the DMF droplets contact angles on the surface of the BT-MTP (A) and DFBT-MTP (B) film; images of the water droplets contact angles on the surface of the BT-MTP (C) and DFBT-MTP (D) film.

5. The SCLC measurement

The hole-transport mobility of BT-MTP and DFBT-MTP were measured by the SCLC technique. The ITO/PEDOT:PSS/dopant-free HTMs/MoO_3/Al-structured device were fabricated, and the HTM layers were fabricated as same as the corresponding PVK-SCs. the hole mobility of HTMs were measured under dark conditions and the values were calculated using the Mott–Gurney law:

$$J = \frac{9}{8}\varepsilon_r \varepsilon_0 \mu \frac{v^2}{L^3}$$

6. Cross-section SEM images

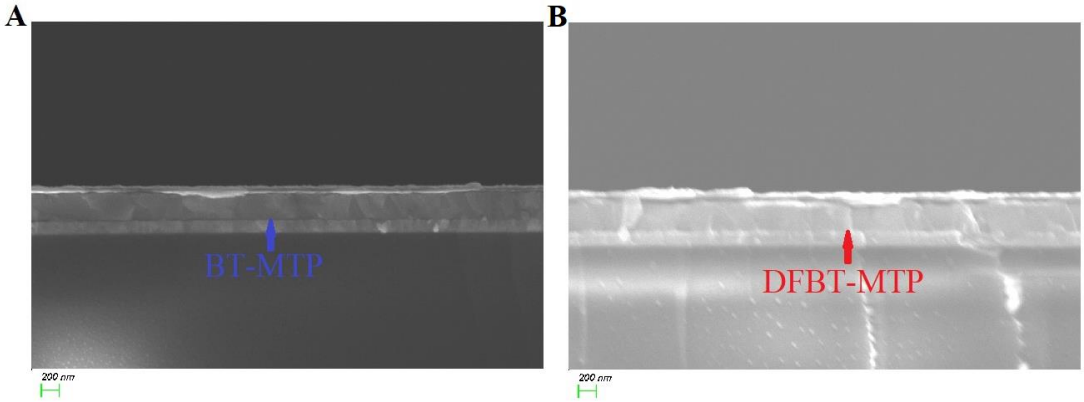

Figure S6. A-B: The Cross-section SEM image of the *p-i-n* PVK-SCs based on BT-MTP and DFBT-MTP, respectively.

7. Performance of the PVK-SCs in different concentrations and annealing time

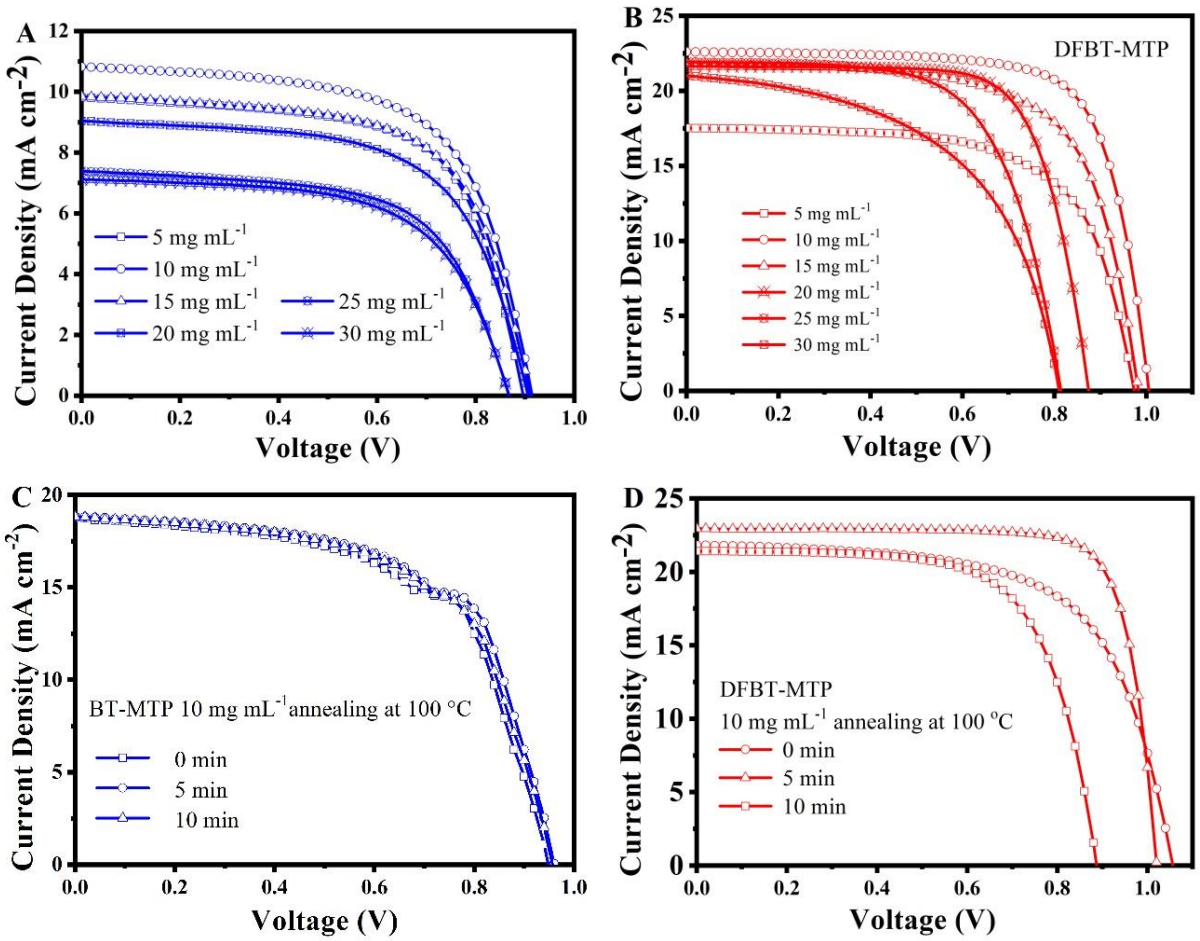

Figure S7. A-B: The *J-V* curves of the *p-i-n* PVK-SCs prepared from different concentrations of BT-MTP and DFBT-MTP solution; C-D: *J-V* curves of the *p-i-n* PVK-SCs prepared from different thermal annealing times at 100 ℃ of BT-MTP and DFBT-MTP films.

Table S2. Photovoltaic performance of the *p-i-n* PVK-SCs with BT-MTP HTL prepared from different concentrations and annealing time under the illumination of AM 1.5G, 100 mW cm^{-2}.

Concentration (mg mL^{-1})	Annealing time (100℃) (min)	*J*sc (mA cm^{-2})	*V*oc (V)	*FF* (%)	PCE (%)
5	0	8.34	0.88	65.63	4.82
10	0	10.83	0.91	63.09	6.25
15	0	9.85	0.91	63.64	5.71
20	0	9.04	0.91	62.36	5.11
25	0	7.39	0.87	62.15	3.99
30	0	7.12	0.87	61.39	3.79
10	0	18.78	0.95	61.20	10.90
10	5	18.84	0.96	62.20	11.26
10 (optimization)	5	20.87	0.97	73.60	14.95
10	10	18.83	0.96	60.20	10.85

Table S3. Photovoltaic performance of the *p-i-n* PVK-SCs with DFBT-MTP HTL prepared from different concentrations and annealing time under the illumination of AM 1.5G, 100 mW cm^{-2}.

Concentration (mg mL^{-1})	Annealing time (100℃) (min)	*J*sc (mA cm^{-2})	*V*oc (V)	*FF* (%)	PCE (%)
5	0	17.54	0.97	65.41	11.17
10	0	22.61	1.00	73.52	16.71
15	0	21.80	0.98	67.09	14.37
20	0	21.64	0.87	72.50	13.73
25	0	21.93	0.81	64.69	11.55
30	0	21.01	0.81	53.25	9.07
10	0	22.61	1.00	73.52	16.71
10	5	22.94	1.02	79.28	18.56
10 (optimization)	5	23.01	1.10	79.68	20.15
10	10	21.41	0.89	67.15	12.76

Table S4. Photovoltaic performance of the PVK-SCs based on BT-MTP and DFBT-MTP in reverse and forward scans under the illumination of AM 1.5G, 100 mW cm^{-2}.

DF-HTMs		*J*sc (mA cm^{-2})	*V*oc (V)	*FF* (%)	PCE (%)
BT-MTP	Forward	20.93	0.96	70.9	14.20
	Reverse	20.87	0.97	73.6	14.95
DFBT-MTP	Forward	22.90	1.08	79.36	19.73
	Reverse	23.01	1.08	79.61	19.88

8. A summary of the reported p-i-n PVK-SCs based on DF-HTMs

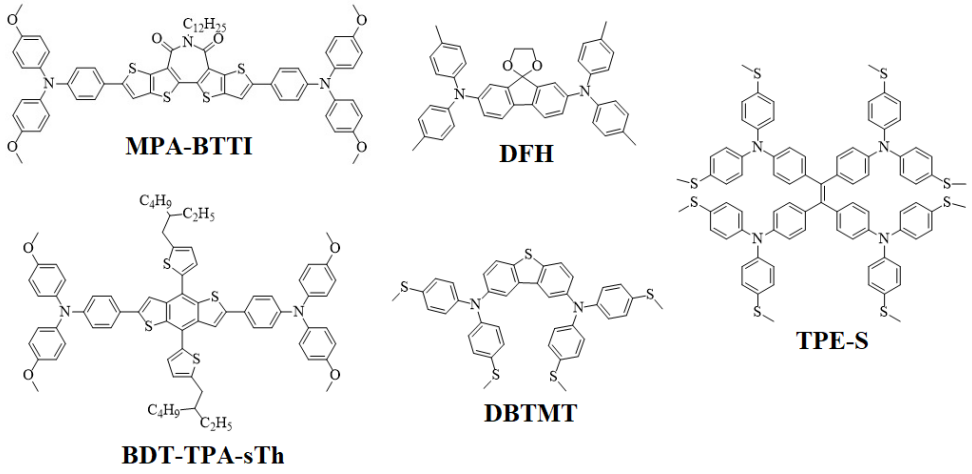

Figure S8. The structures of the DF-HTMs applied for *p-i-n* PVK-SCs with high efficiency reported.

Table S5. The performance parameters of the *p-i-n* PVK-SCs based on DF-HTMs reported.

DF-HTMs (small molecules)	Perovskites	J_{SC} (mA cm^{-2})	*V*oc (V)	*FF* (%)	PCE (%)	Ref (main text)
MPA-BTTI	CsFAMA	23.23	1.12	81.4	21.17	6
DFH	$MA_{0.9}FA_{0.1}PbI_{3-x}Cl_x$	22.7	1.09	83.0	20.6	33
BDT-TPA-sTh	$MAPbI_3$	21.91	1.03	79.02	17.83	34
	SSG-G	22.87	1.15	78	20.5	
DBTMT	$MAPbI_{3-x}Cl_x$	22.7	1.12	83.25	21.12	31
TPE-S	$FA_{0.9}Cs_{0.1}PbI_3$	23.3	1.13	79.7	21.0	11
This work	$MAPbI_{3-x}Cl_x$	23.01	1.10	79.68	20.15	

9. Stability of the PVK-SCs based on BT-MTP

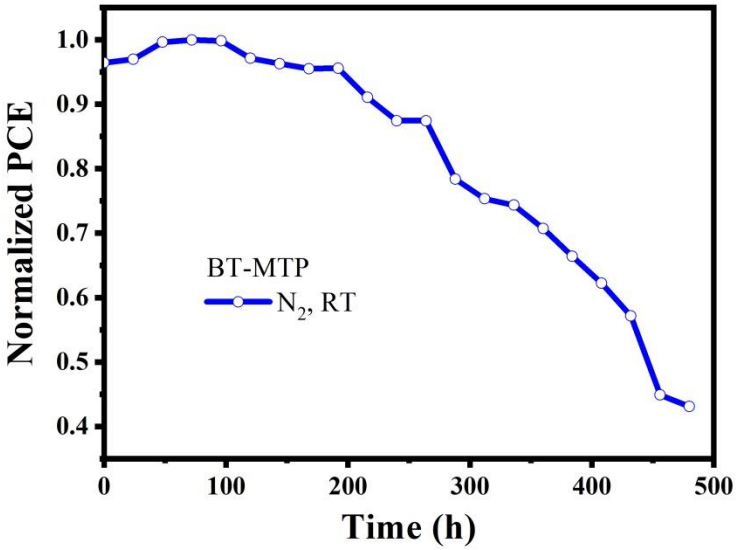

Figure S9. The stability of the PVK-SCs based on BT-MTP in nitrogen ambient at RT.

10. XPS of the core-level of I 3d spectra

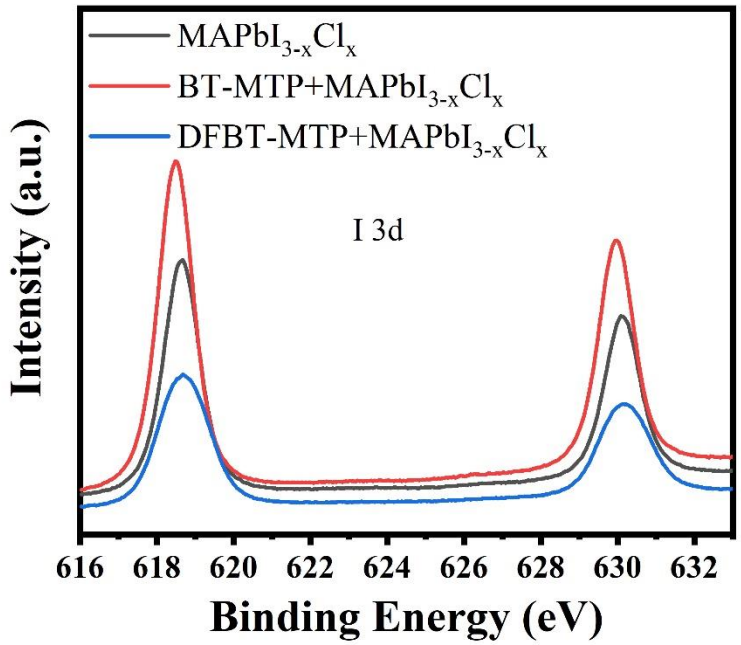

Figure S10. XPS of the core-level of I 3d spectra of $MAPbI_{3-x}Cl_x$@ITO, $MAPbI_{3-x}Cl_x$@BT-MTP and $MAPbI_{3-x}Cl_x$@DFBT-MTP films.

Table S6. The core-level of Pb 4f of $MAPbI_{3-x}Cl_x$@ITO, $MAPbI_{3-x}Cl_x$@BT-MTP and $MAPbI_{3-x}Cl_x$@DFBT-MTP films.

Films	Pb 4f Binding energy (eV)	Pb 4f Binding energy (eV)
$MAPbI_{3-x}Cl_x$@ITO	137.88	142.73
$MAPbI_{3-x}Cl_x$@BT-MTP	137.78	142.63
$MAPbI_{3-x}Cl_x$@DFBT-MTP	137.83	142.72